

Original Article

Loss of Natriuretic Peptide Receptor C Enhances Sinoatrial Node Dysfunction in Aging and Frail Mice

Hailey J. Jansen, PhD,¹ Motahareh Moghtadaei, PhD,¹ Sara A. Rafferty, MSc,² Darrell D. Belke, PhD,¹ and Robert A. Rose, PhD^{1,*}

¹Departments of Cardiac Sciences and Physiology and Pharmacology, Libin Cardiovascular Institute, Cumming School of Medicine, University of Calgary, Calgary, Alberta, Canada. ²Department of Physiology and Biophysics, Faculty of Medicine, Dalhousie University, Halifax, Nova Scotia, Canada.

*Address correspondence to: Robert A. Rose, PhD, Libin Cardiovascular Institute, Cumming School of Medicine, University of Calgary, GAC66, Health Research Innovation Centre, 3280 Hospital Drive N.W., Calgary, AB T2N 4Z6, Canada. E-mail: robert.rose@ucalgary.ca

Received: May 12, 2021; Editorial Decision Date: November 19, 2021

Decision Editor: Rozalyn M. Anderson, PhD, FGSA

Abstract

Heart rate (HR) is controlled by the sinoatrial node (SAN). SAN dysfunction is highly prevalent in aging; however, not all individuals age at the same rate. Rather, health status during aging is affected by frailty. Natriuretic peptides regulate SAN function in part by activating natriuretic peptide receptor C (NPR-C). The impacts of NPR-C on HR and SAN function in aging and as a function of frailty are unknown. Frailty was measured in aging wild-type and NPR-C knockout (NPR-C^{-/-}) mice using a mouse clinical frailty index (FI). HR and SAN structure and function were investigated using intracardiac electrophysiology in anesthetized mice, high-resolution optical mapping in intact atrial preparations, histology, and molecular biology. NPR-C^{-/-} mice rapidly became frail leading to shortened life span. HR was reduced and SAN recovery time was increased in older versus younger mice, and these changes were exacerbated in NPR-C^{-/-} mice; however, there was substantial variability among age groups and genotypes. HR and SAN recovery time were correlated with FI score and fell along a continuum regardless of age or genotype. Optical mapping demonstrates impairments in SAN function that were also correlated with FI score. SAN fibrosis was increased in aged and NPR-C^{-/-} mice and was graded by FI score. Loss of NPR-C results in accelerated aging and rapid decline in health status in association with impairments in HR and SAN function. Frailty assessment was effective and better able to distinguish aging-dependent changes in SAN function in the setting of shortened life span due to loss of NPR-C.

Keywords: Aging, Electrophysiology, Fibrosis, Frailty, Heart rate

Heart rate (HR) is determined by the intrinsic pacemaker activity of the sinoatrial node (SAN) and is a major determinant of cardiac performance (1, 2). SAN dysfunction is prominent in aging populations with an incidence of 1 in 600 patients older than the age of 65 (3–5). SAN dysfunction results in HRs that are insufficient to meet the physiological requirements of the body and can lead to artificial pacemaker implantation (3).

The SAN contains specialized myocytes that generate spontaneous action potentials (APs) characterized by the presence of a diastolic depolarization (DD) between successive APs (1, 2). The DD is generated by several ionic currents including the hyperpolarization-activated current (generated by HCN channels) and L-type Ca²⁺ currents (generated by Ca_v1.2 and Ca_v1.3 channels) among others (1, 2). The rate of DD is a critical determinant of HR in vivo. Spontaneous

AP firing in the SAN is also affected by interstitial collagen deposition, whereby SAN fibrosis can disrupt SAN electrical conduction and impair the ability of the SAN to activate the surrounding atrial myocardium (6).

While age is clearly a major risk factor for SAN dysfunction, aging is heterogeneous and not all individuals age at the same rate (7). This has led to the concept of frailty, which is described as a state of increased susceptibility to adverse health outcomes (7). Thus, aging individuals can vary in health status from fit to frail. Frailty can be viewed as an accumulation of health deficits over time and can be quantified using a frailty index (FI) (7, 8). We recently developed the mouse clinical FI, which is a noninvasive FI that quantifies frailty based on 31 well-established indicators of overall health status (8). With this approach, the FI score for an

individual is determined by assessing the number of deficits present and dividing by the total number of items assessed to produce an FI score between 0 (no deficits present, least frail) and 1 (all deficits present, most frail). The mouse clinical FI accurately reproduces the features of deficit accumulation and frailty development in aging humans (7). This mouse clinical FI has now been used in numerous studies of aging and frailty in mice (9–13) including to determine the impacts of age and frailty on cardiac function (9–11). We previously showed that SAN structure and function are strongly correlated with FI score in aging mice indicating that SAN dysfunction is dependent on frailty (9, 14).

Natriuretic peptides (NPs) are a family of cardioprotective hormones that play critical roles in regulating cardiac structure and cardiac electrophysiology, including in the SAN (15, 16). Interestingly, studies have shown that circulating levels of NPs, including atrial NP (ANP) and C-type NP (CNP), decline in aging rats and that this is associated with enhanced cardiac fibrosis (17, 18). N-terminal proCNP has also been shown to decline in aging humans (19). These observations suggest that derangements in the NP system could contribute importantly to aging-related cardiac dysfunction. NPs elicit their effects in part by activating NP receptor C (NPR-C), which has high affinity for all NPs (15). NPR-C is highly expressed in the SAN and has previously been shown to regulate HR and SAN function (20–22). The links between NPR-C and SAN function in aging and frail mice are unknown. Accordingly, the purpose of this study was to assess HR and SAN function in wildtype (WT) and NPR-C^{-/-} mice as a function of age and frailty.

Method

An expanded *Method* section is available in [Supplementary Material](#).

Mice

Male and female WT and NPR-C^{-/-} mice were bred and maintained in our local animal facility. All experimental procedures were approved by the University of Calgary Animal Care and Use Committee or the Dalhousie University Committee for Laboratory Animals and conformed to the guidelines of the Canadian Council on Animal Care.

Mouse Clinical Frailty Assessment

Frailty was assessed in mice using the mouse clinical FI as described previously (8, 9) and in [Supplementary Material](#).

In Vivo Electrophysiology

HR and SAN recovery time (SNRT) were measured in anesthetized mice (2% isoflurane inhalation) using surface electrocardiogram recordings and intracardiac electrophysiology as described previously (9, 23) and in [Supplementary Material](#).

High-Resolution Optical Mapping

Electrical conduction in the SAN was measured using high-resolution optical mapping in isolated atrial preparations as described previously (23, 24) and in [Supplementary Material](#).

Quantitative PCR

Gene expression was measured in the SAN as previously described (9, 23). Primer sequences and protocols are provided in [Supplementary Material](#) and in [Supplementary Table 1](#).

Sinoatrial Node Fibrosis

Fibrosis in the SAN was assessed histologically as described previously (23) and in [Supplementary Material](#).

Statistical Analysis

Data are presented as mean ± SEM. Data were analyzed using a Student’s *t*-test, 2-way analysis of variance with a Tukey post hoc test, or log-rank test as indicated in each figure legend. Frailty analyses were performed by linear regression analysis and Pearson correlations. In all cases, *p* < .05 was considered significant.

Results

Frailty and Survival in Aging WT and NPR-C^{-/-} Mice

FI scores were measured longitudinally in WT and NPR-C^{-/-} mice beginning at 20 weeks of age ([Figure 1A](#)). WT mice were aged up

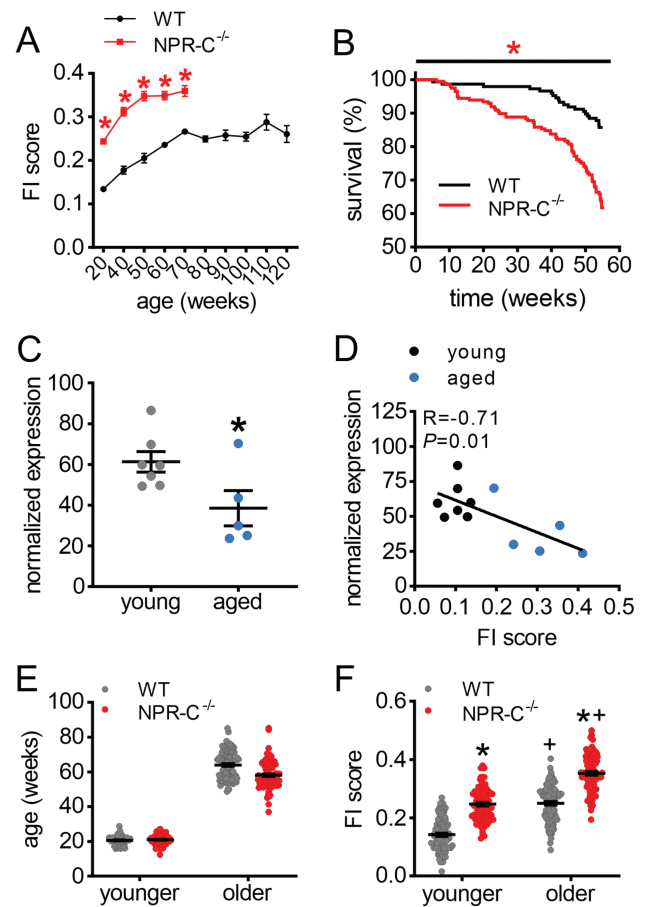


Figure 1. Loss of NPR-C increases frailty and impairs survival in aging mice. (A) Changes in frailty index (FI) score in aging WT and NPR-C^{-/-} mice. **p* < .05 versus WT by 2-way repeated-measures analysis of variance (ANOVA). (B) 1-year survival curve for WT (*n* = 126) and NPR-C^{-/-} (*n* = 122) mice. **p* < .05 versus WT by log-rank test. (C) mRNA expression of *npr3* (NPR-C) in young (10–12 weeks; *n* = 7) and aged (87–117 weeks; *n* = 5) WT mice. **p* < .05 versus young by Student’s *t*-test. (D) Expression of *npr3* as a function of FI score (same mice as panel C). (E) Ages of younger and older WT and NPR-C^{-/-} mice that were used to evaluate sinoatrial node function in this study. (F) FI scores in younger and older WT and NPR-C^{-/-} mice (same mice as panel E); **p* < .05 versus WT, +*p* < .05 versus younger by 2-way ANOVA with a Tukey post hoc test. For panels E and F, *n* = 97 mice for WT younger, 104 for WT older, 82 for NPR-C^{-/-} younger, and 100 for NPR-C^{-/-} older. NPR-C = natriuretic peptide receptor C.

to 120 weeks and FI scores increased over time as expected (8, 9). In contrast, NPR-C^{-/-} mice had higher FI scores than WT mice and reached maximum FI scores by 70 weeks of age. Survival at 1 year was reduced in NPR-C^{-/-} mice (Figure 1B), and no NPR-C^{-/-} mice survived past ~80 weeks of age. Thus, loss of NPR-C results in shortened life span in association with the more rapid accumulation of aging-related frailty. Expression of *npr3* (encodes NPR-C) was reduced in the SAN of aged WT mice compared to young WT mice (Figure 1C) and as a function of FI score (Figure 1D).

As a result of the shortened life span in aging NPR-C^{-/-} mice, we investigated SAN function in younger (~20 weeks) and older (~60 weeks) groups of WT and NPR-C^{-/-} mice so that mice of approximately the same chronological age could be studied (Figure 1E). On average, FI scores were higher in older mice compared to younger mice, and FI scores were also elevated in NPR-C^{-/-} mice in both age groups (Figure 1F). Notably, there was a range of FI scores within each group and substantial overlap was apparent indicating differences in health status within age and genotype groups. Ages and FI scores were comparable between male and female WT and NPR-C^{-/-} mice (Supplementary Figure 1).

HR and Sinoatrial Node Function in Aging WT and NPR-C^{-/-} Mice

HR was reduced in older versus younger WT mice and in younger NPR-C^{-/-} mice versus younger WT mice; however, differences in HR were not detected in older NPR-C^{-/-} mice compared to older WT or younger NPR-C^{-/-} mice (Figure 2A and B). Similarly, corrected SAN recovery time (cSNRT) was increased in older versus younger mice of both genotypes and in NPR-C^{-/-} mice versus WT mice at both ages (Figure 2C). Notably, there was substantial variability within each age group and genotype (Figure 2B and C), suggesting factors other than chronological age affect SAN function. When HR was plotted as a function of frailty for all mice studied, HR and cSNRT were strongly correlated with FI score (Figure 2D and E), whereby HR and cSNRT fell along a continuum as a function of frailty. The effects of age and frailty on HR and cSNRT were similar between male and female mice (Supplementary Figure 2).

Measurement of intrinsic HR (ie, HR as determined by intrinsic SAN function) after autonomic nervous system blockade was also reduced in older WT and NPR-C^{-/-} mice compared to younger mice; however, differences between NPR-C^{-/-} mice and WT mice within age groups were not detected (Supplementary Figure 3). Nevertheless, intrinsic HR showed strong negative correlations with FI score (Supplementary Figure 3).

Cardiac Structure and Plasma Creatinine

Overall, there were few changes in left ventricular anterior wall (Supplementary Figure 4A–C) and posterior wall (Supplementary Figure 4D and E) thickness, or left ventricular internal diameter (Supplementary Figure 4F and G), as a function of age and genotype and none as a function of FI score. There were also no differences in fractional shortening or ejection fraction as a function of age and genotype or FI score (Supplementary Figure 4H and I).

Body mass was increased in older WT mice compared to younger WT mice, while body mass in older NPR-C^{-/-} mice was not different from younger NPR-C^{-/-} mice (Supplementary Figure 5), indicating that NPR-C^{-/-} mice did not gain as much mass during aging. No differences were seen in plasma creatinine when measured as a function of age and genotype; however, plasma creatinine was negatively correlated with FI score (Supplementary Figure 6).

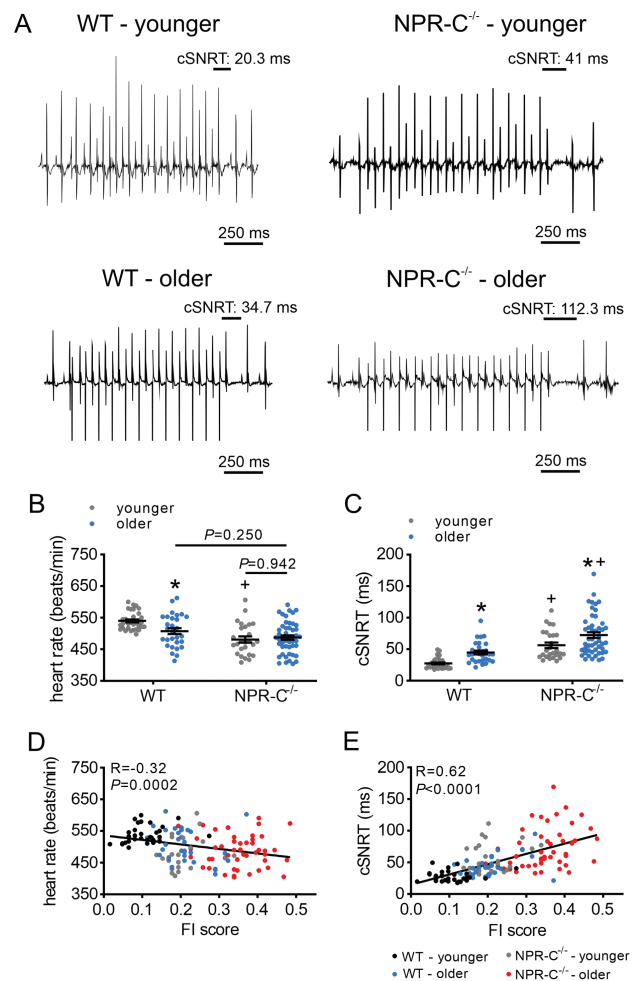


Figure 2. Effects of age and frailty on sinoatrial node function in WT and NPR-C^{-/-} mice in vivo. (A) Representative recordings illustrating corrected sinoatrial node recovery time (cSNRT) in younger and older WT and NPR-C^{-/-} mice. (B and C) Heart rate (B) and cSNRT (C) in younger and older WT and NPR-C^{-/-} mice (males and females combined). **p* < .05 versus younger, †*p* < .05 versus WT by 2-way analysis of variance with a Tukey post hoc test. (D and E) Heart rate (D) and cSNRT (E) as a function of FI score for younger and older WT and NPR-C^{-/-} mice (same mice as panels B and C). *n* = 32 mice for WT younger, 29 for WT older, 26 for NPR-C^{-/-} younger, and 48 for NPR-C^{-/-} older. NPR-C = natriuretic peptide receptor C.

SAN Electrical Conduction in Aging WT and NPR-C^{-/-} Mice

Activation maps and plots of initial activation sites in the SAN demonstrate that, as expected, the majority of younger WT mice had initial activation sites in the region of the right atrial posterior wall adjacent to the crista terminalis, which corresponds to the location of the SAN (Figure 3A). In contrast, the other groups exhibited substantial variability in the location of the leading activation site, particularly the older NPR-C^{-/-} mice (Figure 3A). When analyzed as a function of frailty, the initial activation site was consistently in the superior region of the SAN in the least frail mice while mice with higher FI scores displayed variability in the location of the leading activation site (Figures 3B). Beating rate in atrial preparations was reduced in older versus younger WT mice and in younger NPR-C^{-/-} mice versus younger WT mice (Figure 3C and D); however, differences were not detected for older NPR-C^{-/-} mice which displayed substantial variability. Beating rate fell on a continuum and was

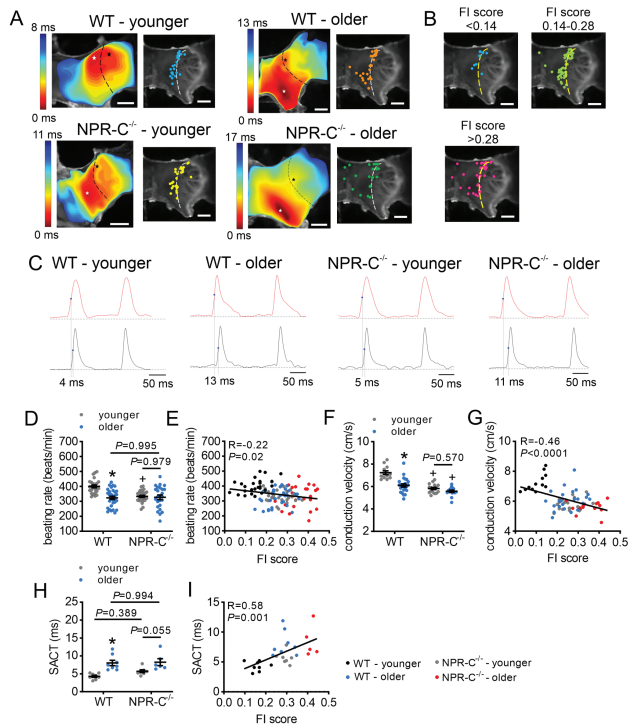


Figure 3. Effects of age and frailty on sinoatrial node electrical conduction in WT and NPR-C^{-/-} mice. (A) Representative activation maps (left) and leading activation sites (right) in younger and older WT and NPR-C^{-/-} mice. Right atrium is on the right side of the images. Dashed lines indicate crista terminalis. Red color on activation maps indicates the earliest activation time. (B) Leading activation sites as a function of FI score bins. (C) Optical action potentials (OAPs) from the initial activation site (white asterisk on activation map) and the earliest right atrial activation site (black asterisk on activation map) for younger and older WT and NPR-C^{-/-} mice. Values indicated by vertical lines are the sinoatrial node to atrial conduction times (SACT). (D) Beating rate in younger and older WT and NPR-C^{-/-} mice; *n* = 25 mice for WT younger, 31 for WT older, 29 for NPR-C^{-/-} younger, and 24 for NPR-C^{-/-} older. (E) Beating rate as a function of FI score for younger and older WT and NPR-C^{-/-} mice (same mice as panel D). (F) Conduction velocity in the right atrial posterior wall in younger and older WT and NPR-C^{-/-} mice, *n* = 12 mice for WT younger, 23 for WT older, 17 for NPR-C^{-/-} younger, and 16 for NPR-C^{-/-} older. (G) Conduction velocity as a function of FI score for younger and older WT and NPR-C^{-/-} mice (same mice as panel F). (H) SACT for younger and older WT and NPR-C^{-/-} mice, *n* = 8 mice for WT younger, 8 for WT older, 7 for NPR-C^{-/-} younger, and 6 for NPR-C^{-/-} older. (I) SACT as a function of FI score for younger and older WT and NPR-C^{-/-} mice (same mice as panel H). For panels D, F, and H, **p* < .05 versus younger, **p* < .05 versus wildtype by 2-way analysis of variance with a Tukey post hoc test. NPR-C = natriuretic peptide receptor C.

negatively correlated with FI score (Figure 3E). Conduction velocity in the SAN region of the right atrial posterior wall was reduced in older versus younger WT mice and in NPR-C^{-/-} mice versus WT mice; however, differences were not detected in older versus younger NPR-C^{-/-} mice (Figure 3F). Conduction velocity was negatively correlated with FI score (Figure 3G).

Activation maps (Figure 3A) and optical APs (OAPs) from the SAN and the adjacent right atrial free wall (Figure 3C) were also used to assess SAN to atrial conduction time (SACT). SACT was prolonged in older versus younger WT mice with similar trends for older versus younger NPR-C^{-/-} mice; however, differences were not detected for NPR-C^{-/-} mice compared to WT mice (Figure 3H). SACT was also correlated with FI score (Figure 3I).

OAP (Figure 4A) analysis also shows that DD slope was reduced in older versus younger mice, and in NPR-C^{-/-} mice versus WT mice

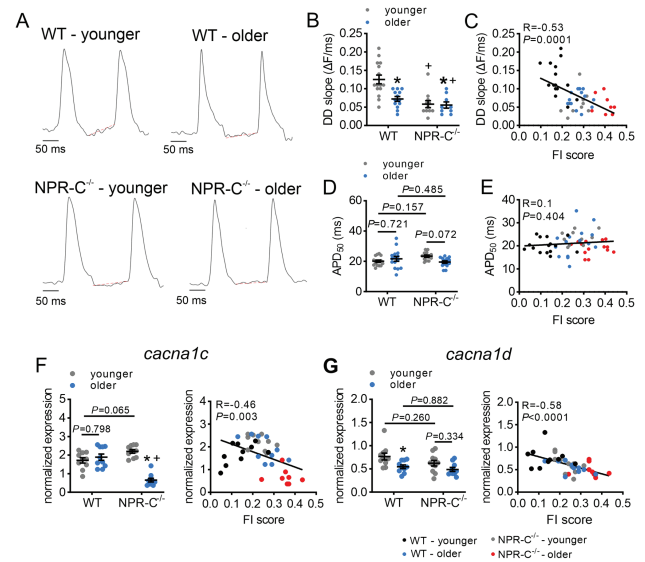


Figure 4. Effects of age and frailty on sinoatrial node action potential morphology in WT and NPR-C^{-/-} mice. (A) Representative sinoatrial node spontaneous optical action potentials in younger and older WT and NPR-C^{-/-} mice. Red lines represent linear fitting of the diastolic depolarization (DD). (B) DD slope in younger and older WT and NPR-C^{-/-} mice, *n* = 15 mice for WT younger, 13 for WT older, 11 for NPR-C^{-/-} younger, and 9 for NPR-C^{-/-} older. (C) DD slope as a function of FI score for younger and older WT and NPR-C^{-/-} mice (same mice as panel B). (D) Action potential duration at 50% repolarization (APD₅₀) in younger and older WT and NPR-C^{-/-} mice, *n* = 15 mice for WT younger, 15 for WT older, 13 for NPR-C^{-/-} younger, and 15 for NPR-C^{-/-} older. (E) APD₅₀ as a function of FI score in younger and older WT and NPR-C^{-/-} mice (same mice as panel D). (F) mRNA expression of *cacna1c* in younger and older WT and NPR-C^{-/-} mice (left panel) and as a function of FI score (right panel); *n* = 10 mice for WT younger, 10 for WT older, 10 for NPR-C^{-/-} younger, and 10 for NPR-C^{-/-} older. (G) mRNA expression of *cacna1d* in younger and older WT and NPR-C^{-/-} mice (left panel) and as a function of FI score (right panel); *n* = 10 mice for WT younger, 10 for WT older, 11 for NPR-C^{-/-} younger, and 10 for NPR-C^{-/-} older. For figures as a function of chronological age and genotype, **p* < .05 versus younger; **p* < .05 versus WT by 2-way analysis of variance with a Tukey post hoc test. NPR-C = natriuretic peptide receptor C.

(Figure 4B), and negatively correlated with FI score (Figure 4C). AP duration at 50% repolarization (APD₅₀) was not altered as a function of chronological age or genotype (Figure 3D) or as a function of FI score (Figure 3E).

The mRNA expression of *cacna1c* (encodes Ca_v1.2) in the SAN was reduced in older NPR-C^{-/-} mice compared to younger NPR-C^{-/-} mice and older WT mice (Figure 4F); however, differences among other groups were not observed. Nevertheless, expression of *cacna1c* was negatively correlated with FI score (Figure 4F). The expression of *cacna1d* (encodes Ca_v1.3) was reduced in older versus younger WT mice, while differences in other groups were not detected (Figure 4G). *Cacna1d* expression was also negatively correlated with FI score (Figure 4G). There were no differences in expression of *hcn1*, *hcn2*, or *hcn4* as a function of age and genotype or as a function of FI score in the SAN (Supplementary Figure 7).

Sinoatrial Node Fibrosis in Aging WT and NPR-C^{-/-} Mice

SAN fibrosis was increased in older versus younger WT mice and in younger NPR-C^{-/-} mice versus younger WT mice; however, no differences were detected in older NPR-C^{-/-} mice compared to other

groups (Figure 5A and B). Despite this, SAN fibrosis was correlated with FI score (Figure 5C).

While differences in the mRNA expression of *timp1* in the SAN did not show differences as a function of age or genotype, *timp1* expression was clearly correlated with FI score (Figure 5D). The mRNA expression of *mmp9* did not exhibit differences among age groups or as a function of FI (Figure 5E); however, remodeling of the extracellular matrix is affected by the balance between TIMP and MMP activity. Accordingly, the ratio of *timp1* to *mmp9* expression was also quantified (Figure 5F). *Timp1/mmp9* ratio in the SAN was strongly correlated with FI score. Other genes involved in fibrotic signaling, including *col1a* (encodes collagen type I), *col3a* (encodes collagen type III), *tgfb1* (encodes TGF β), *timp2*, *timp3*, and *timp4* were not altered in different age groups or as a function of frailty (Supplementary Figure 8).

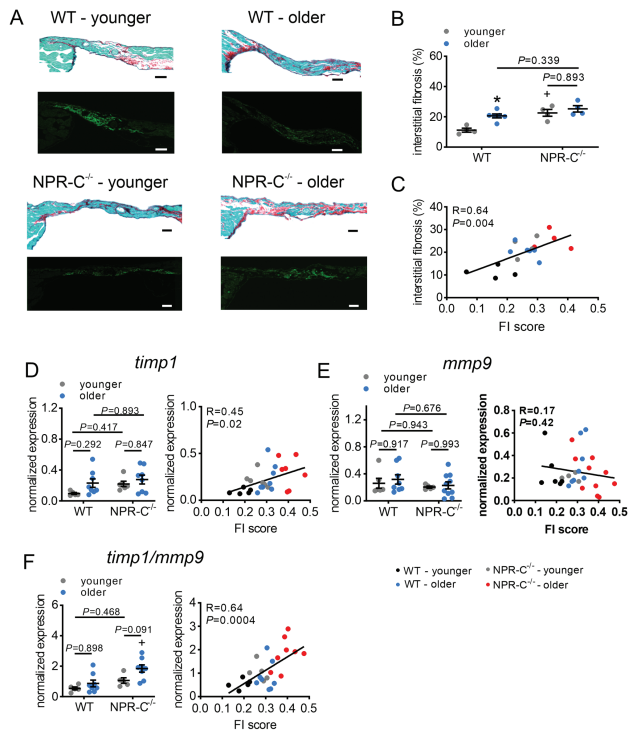


Figure 5. Effects of age and frailty on sinoatrial node fibrosis in WT and NPR-C^{-/-} mice. (A) Representative sections through the sinoatrial node in younger and older WT and NPR-C^{-/-} mice. Top panels illustrate picosirius red staining to identify fibrosis (collagen stained red). Bottom panels illustrate the HCN4-positive zone (green) to confirm the location of the sinoatrial node. Scale bars = 50 μ m. (B) Sinoatrial node interstitial fibrosis in younger and older WT and NPR-C^{-/-} mice. $n = 4$ mice for WT younger, 6 for WT older, 4 for NPR-C^{-/-} younger, and 4 for NPR-C^{-/-} older. (C) Sinoatrial node fibrosis in younger and older WT and NPR-C^{-/-} mice as a function of FI score (same mice as panel B). (D) mRNA expression of *timp1* in younger and older WT and NPR-C^{-/-} mice (left panel) and as a function of FI score (right panel); $n = 5$ mice for WT younger, 8 for WT older, 6 for NPR-C^{-/-} younger, and 8 for NPR-C^{-/-} older. (E) mRNA expression of *mmp9* in younger and older WT and NPR-C^{-/-} mice (left panel) and as a function of FI score (right panel); $n = 6$ mice for WT younger, 8 for WT older, 5 for NPR-C^{-/-} younger, and 10 for NPR-C^{-/-} older. (F) Ratio of expression of *timp1/mmp9* in younger and older WT and NPR-C^{-/-} mice (left panel) and as a function of FI score (right panel); $n = 5$ mice for WT younger, 8 for WT older, 5 for NPR-C^{-/-} younger, and 8 for NPR-C^{-/-} older. For figures as a function of chronological age and genotype, * $p < .05$ versus younger; * $p < .05$ versus WT by 2-way analysis of variance with a Tukey post hoc test. NPR-C = natriuretic peptide receptor C.

Discussion

Here we show that NPR-C^{-/-} mice rapidly become frail leading to a shortened life span in association with enhanced development of aging-dependent SAN dysfunction. NPR-C^{-/-} mice displayed enhanced mortality at 1 year of age and no NPR-C^{-/-} mice survived past ~80 weeks (~18 months) of age. FI scores were higher in NPR-C^{-/-} mice at all time points and reached maximum values at 50–80 weeks of age when these mice either died or had to be euthanized for humane reasons. In contrast, WT mice did not reach similar FI scores until ~120 weeks (~27 months) of age, as expected (9, 10). Consistent with this, we also found that expression of NPR-C in the SAN was reduced in aged WT mice and as a function of FI score, further indicating that changes in NPR-C expression are associated with frailty development in aging mice. Importantly, the mouse clinical FI provides an assessment of overall health status by quantifying general indicators of health across several organ systems during the aging process (7, 8). As such, FI scores are strongly associated with health status and risk of mortality in aging mice (7). The observation that FI scores were increased in NPR-C^{-/-} mice in association with increased mortality indicates that the shortened life span in these mice occurs due to accelerated aging and a more rapid decline in health status. These findings support the conclusion that NPs and NPR-C play a critical role in maintaining HR and SAN function, and that these correlate with frailty (ie, health status) in aging.

Declining cardiac function is a major component of aging-related disease, and HR regulation is central to this as SAN dysfunction is recognized as a key contributor to the aging-related loss of cardiac performance (3, 4). Consistent with this, reductions in intrinsic HR (ie, HR as determined by SAN function) have been demonstrated in aging humans and animal models (25–31). Furthermore, we previously demonstrated that frailty is a strong predictor of SAN dysfunction in aged WT mice (2–2.5 years) (9, 14). We have now identified a critical role for NPR-C in regulating aging-dependent changes in SAN function and HR control and show that frailty can very accurately predict HR and SAN function in aging WT and NPR-C^{-/-} mice. Indeed, while changes were evident among different age groups and genotypes, there was also substantial heterogeneity within groups in a number of measures of SAN function. As a result, differences in HR and SAN function (eg, HR in vivo, beating rate in isolated atrial preparations, SAN conduction velocity, SACT) were not always detected among the different groups of mice. Despite this, frailty analysis showed that these measures of SAN function were strongly correlated with FI score. Linear regressions clearly demonstrate that measurements of HR and SAN function fell along a continuum and were graded by FI score, indicating that frailty can be a better determinant of changes in SAN function in aging WT and NPR-C^{-/-} mice. From this, it is evident that HR and SAN function are importantly associated with overall health status and that frailty can accurately predict SAN function regardless of age or genotype.

SAN dysfunction can develop due to an inability of pacemaker myocytes to generate and conduct spontaneous APs (3, 6). Consistent with this, we found that conduction velocity and SACT were impaired in aging WT and NPR-C^{-/-} mice in association with a reduction in DD slope. Furthermore, DD slope was strongly correlated with FI score indicating that this is an important contributor to aging-dependent changes in SAN function and that this is exacerbated by a loss of NPR-C. We found that *cacna1c* and *cacna1d*, the genes encoding Ca_v1.2 and Ca_v1.3, respectively, were strongly negatively correlated with FI score. Ca_v1.2 and Ca_v1.3 both underlie the L-type Ca²⁺ current in SAN myocytes (1). Ca_v1.2 is importantly

involved in generating the AP upstroke, while $Ca_v1.3$ is a major determinant of DD slope in SAN myocytes (1). Reduced expression of both genes could therefore lead to smaller $I_{Ca,L}$ in SAN myocytes and contribute importantly to the slower beating rate, reduced conduction velocity, and prolonged SACT in frail mice. Frailty was a better predictor of changes in Ca^{2+} channel gene expression than chronological age and genotype, which is consistent with the functional alterations identified in this study. Additional studies will be needed to further investigate the role of $I_{Ca,L}$ in frailty-dependent SAN dysfunction.

SAN conduction is also critically affected by the amount of interstitial collagen in the SAN (6). Increased collagen deposition leading to fibrosis can slow or disrupt conduction within the SAN and from the SAN to the atrium. SAN fibrosis has been previously shown in the aging heart (9, 32–34). Furthermore, NPR-C has been shown to control SAN fibrosis in young adult mice (20, 23). Consistent with these findings, the present study demonstrates that SAN fibrosis in aging WT and NPR-C^{-/-} mice is strongly correlated with FI score. Gene expression studies demonstrate changes that could underlie SAN fibrosis. Notably, *timp1* and the ratio of *timp1/mmp9* expression were each strongly correlated with FI score in aging WT and NPR-C^{-/-} mice. Frailty was better able to distinguish these changes in expression compared to changes as function of age and genotype. Increasing *timp1* expression as a function of frailty could contribute to SAN fibrosis in several ways. Specifically, TIMP1 has been shown to enhance collagen deposition independently of its inhibitory effects on MMPs (35). TIMP1 can also change the balance between MMP and TIMP activity (as suggested by the ratio of *timp1/mmp9* expression), which could contribute to fibrosis by causing the retention of collagens in the extracellular matrix (36). MMP9 was considered as it is expressed in the SAN and plays an important role in extracellular matrix remodeling in the heart (9). Further studies will be required to determine the specific role and mechanisms by which TIMP1 and MMPs affect SAN fibrosis in aging and frail mice.

No major differences in ventricular structure were observed in NPR-C^{-/-} mice compared to wildtypes as a function of age or frailty, suggesting no alterations in cardiac structure in association with slower HR. Similarly, body mass was not correlated with FI scores. This is consistent with the direct effects of NPR-C in the SAN where it is highly expressed (20, 37). NPR-C is also expressed in renal glomeruli (38); therefore, plasma creatinine was measured as an indicator of kidney function. No differences were seen between age groups, although creatinine levels were negatively correlated with FI score. Collectively, these data suggest that NPR-C^{-/-} mice do not exhibit kidney failure, which is consistent with previous studies showing NPR-C^{-/-} mice maintain an ability to produce dilute urine (38). NPR-C is also expressed in other tissues such as vascular endothelium and smooth muscle (16). It will also be important to investigate whether function in these other tissues is altered as a function of age and frailty.

Previous studies have shown that circulating levels of NPs are not different between NPR-C^{-/-} and WT mice (although the half-life of ANP is increased) (20, 38). Thus, the findings in this study support the conclusion that loss of NPR-C enhances aging-dependent SAN dysfunction due to direct effects in the SAN and that these alterations are strongly correlated with frailty. Consistent with this, it has recently been shown that loss of NPR-C also enhances aging-dependent atrial fibrillation and atrial dysfunction (39). While studies have shown that circulating ANP and CNP levels are reduced in aging rats (17, 18), and circulating N-terminal proCNP is reduced in aging humans (19), other studies have reported increases

in circulating ANP and BNP in aging humans (40, 41). Thus, additional studies will be needed to determine how changes in circulating NPs, as well as changes in NP receptor expression, collectively contribute to aging and frailty-dependent changes in health and cardiac function.

In summary, the present study demonstrates a critical role for NPR-C in aging-dependent changes in frailty and survival as well as in the regulation of SAN structure and function during the aging process. Heterogeneity in aging represents a substantial challenge for understanding the occurrence and progression of SAN dysfunction and its treatment in aging populations. Our study illustrates that frailty assessment is a very powerful and effective approach for dealing with this heterogeneity and that an FI can be used to assess changes in HR control and SAN function independently of chronological age including in the setting of accelerated aging due to genetic ablation of NPR-C. Based on these findings, NPR-C may be considered as a target for improving health status and maintaining SAN structure and function in aging and frail patients.

Supplementary Material

Supplementary data are available at *The Journals of Gerontology, Series A: Biological Sciences and Medical Sciences* online.

Funding

This work was supported by the Heart and Stroke Foundation of Canada (grant number G-18-0022148) and the Canadian Institutes of Health Research (grant numbers PJT 166105 and MOP 142486) to R.A.R. H.J.J. was supported by a Killam Postdoctoral Fellowship and a Libin Cardiovascular Institute Postdoctoral Fellowship.

Conflict of Interest

None declared.

Author Contributions

H.J.J., M.M., and R.A.R. conceived the study and designed the experiments. H.J.J., M.M., S.A.R., and D.D.B. conducted experiments and analyzed data. H.J.J. and R.A.R. wrote the manuscript. All authors approved the manuscript.

References

1. Mangoni ME, Nargeot J. Genesis and regulation of the heart automaticity. *Physiol Rev*. 2008;88(3):919–982. doi:10.1152/physrev.00018.2007
2. MacDonald EA, Rose RA, Quinn TA. Neurohumoral control of sinoatrial node activity and heart rate: insight from experimental models and findings from humans. *Front Physiol*. 2020;11:170. doi:10.3389/fphys.2020.00170
3. Dobrzynski H, Boyett MR, Anderson RH. New insights into pacemaker activity: promoting understanding of sick sinus syndrome. *Circulation*. 2007;115(14):1921–1932. doi:10.1161/CIRCULATIONAHA.106.616011
4. Lakatta EG, Levy D. Arterial and cardiac aging: major shareholders in cardiovascular disease enterprises: part II: the aging heart in health: links to heart disease. *Circulation*. 2003;107(2):346–354. doi:10.1161/01.cir.0000048893.62841.f7
5. Monfredi O, Boyett MR. Sick sinus syndrome and atrial fibrillation in older persons—a view from the sinoatrial nodal myocyte. *J Mol Cell Cardiol*. 2015;83:88–100. doi:10.1016/j.yjmcc.2015.02.003
6. Csepe TA, Kalyanasundaram A, Hansen BJ, Zhao J, Fedorov VV. Fibrosis: a structural modulator of sinoatrial node physiology and dysfunction. *Front Physiol*. 2015;6:37. doi:10.3389/fphys.2015.00037

7. Rockwood K, Blodgett JM, Theou O, et al. A frailty index based on deficit accumulation quantifies mortality risk in humans and in mice. *Sci Rep*. 2017;7:43068. doi:10.1038/srep43068
8. Whitehead JC, Hildebrand BA, Sun M, et al. A clinical frailty index in aging mice: comparisons with frailty index data in humans. *J Gerontol A Biol Sci Med Sci*. 2014;69(6):621–632. doi:10.1093/gerona/glt136
9. Moghtadaei M, Jansen HJ, Mackasey M, et al. The impacts of age and frailty on heart rate and sinoatrial node function. *J Physiol*. 2016;594(23):7105–7126. doi:10.1113/JP272979
10. Jansen HJ, Moghtadaei M, Mackasey M, et al. Atrial structure, function and arrhythmogenesis in aged and frail mice. *Sci Rep*. 2017;7:44336. doi:10.1038/srep44336
11. Feridooni HA, Kane AE, Ayaz O, et al. The impact of age and frailty on ventricular structure and function in C57BL/6J mice. *J Physiol*. 2017;595(12):3721–3742. doi:10.1113/JP274134
12. Keller K, Kane A, Heinze-Milne S, Grandy SA, Howlett SE. Chronic treatment with the ACE inhibitor enalapril attenuates the development of frailty and differentially modifies pro- and anti-inflammatory cytokines in aging male and female C57BL/6 mice. *J Gerontol A Biol Sci Med Sci*. 2018;74:1149–1157. doi:10.1093/gerona/gly219
13. Chellappa K, Brinkman JA, Mukherjee S, et al. Hypothalamic mTORC2 is essential for metabolic health and longevity. *Aging Cell*. 2019;18(5):e13014. doi:10.1111/acel.13014
14. Dorey TW, Jansen HJ, Moghtadaei M, Jamieson KL, Rose RA. Impacts of frailty on heart rate variability in aging mice: roles of the autonomic nervous system and sinoatrial node. *Heart Rhythm*. 2021;18(11):1999–2008. doi:10.1016/j.hrthm.2021.07.069
15. Moghtadaei M, Polina I, Rose RA. Electrophysiological effects of natriuretic peptides in the heart are mediated by multiple receptor subtypes. *Prog Biophys Mol Biol*. 2016;120(1–3):37–49. doi:10.1016/j.pbiomolbio.2015.12.001
16. Rose RA, Giles WR. Natriuretic peptide C receptor signalling in the heart and vasculature. *J Physiol*. 2008;586(2):353–366. doi:10.1113/jphysiol.2007.144253
17. Sangaralingham SJ, Huntley BK, Martin FL, et al. The aging heart, myocardial fibrosis, and its relationship to circulating C-type natriuretic peptide. *Hypertension*. 2011;57(2):201–207. doi:10.1161/HYPERTENSIONAHA.110.160796
18. Sangaralingham SJ, Wang BH, Huang L, et al. Cardiorenal fibrosis and dysfunction in aging: imbalance in mediators and regulators of collagen. *Peptides*. 2016;76:108–114. doi:10.1016/j.peptides.2016.01.004
19. Keng BMH, Gao F, Tan RS, et al. N-Terminal pro C-type natriuretic peptide (NTproCNP) and myocardial function in ageing. *PLoS One*. 2018;13(12):e0209517. doi:10.1371/journal.pone.0209517
20. Egom EE, Vella K, Hua R, et al. Impaired sinoatrial node function and increased susceptibility to atrial fibrillation in mice lacking natriuretic peptide receptor C. *J Physiol*. 2015;593(5):1127–1146. doi:10.1113/jphysiol.2014.283135
21. Jansen HJ, Mackasey M, Moghtadaei M, et al. NPR-C (natriuretic peptide receptor-C) modulates the progression of angiotensin II-mediated atrial fibrillation and atrial remodeling in mice. *Circ Arrhythm Electrophysiol*. 2019;12(1):e006863. doi:10.1161/CIRCEP.118.006863
22. Azer J, Hua R, Krishnaswamy PS, Rose RA. Effects of natriuretic peptides on electrical conduction in the sinoatrial node and atrial myocardium of the heart. *J Physiol*. 2014;592(5):1025–1045. doi:10.1113/jphysiol.2013.265405
23. Mackasey M, Egom EE, Jansen HJ, et al. Natriuretic peptide receptor-C protects against angiotensin II-mediated sinoatrial node disease in mice. *JACC Basic Transl Sci*. 2018;3(6):824–843. doi:10.1016/j.jacbs.2018.08.004
24. Bohne LJ, Jansen HJ, Daniel I, et al. Electrical and structural remodeling contribute to atrial fibrillation in type 2 diabetic db/db mice. *Heart Rhythm*. 2021;18(1):118–129. doi:10.1016/j.hrthm.2020.08.019
25. Di Gennaro M, Bernabei R, Sgadari A, Carosella L, Carbonin PU. Age-related differences in isolated rat sinus node function. *Basic Res Cardiol*. 1987;82(6):530–536. doi:10.1007/BF01907222
26. Jones SA, Lancaster MK, Boyett MR. Ageing-related changes of connexins and conduction within the sinoatrial node. *J Physiol*. 2004;560(Pt 2):429–437. doi:10.1113/jphysiol.2004.072108
27. Tellez JO, Mczewski M, Yanni J, et al. Ageing-dependent remodeling of ion channel and Ca²⁺ clock genes underlying sino-atrial node pacemaking. *Exp Physiol*. 2011;96(11):1163–1178. doi:10.1113/expphysiol.2011.057752
28. Larson ED, St Clair JR, Sumner WA, Bannister RA, Proenza C. Depressed pacemaker activity of sinoatrial node myocytes contributes to the age-dependent decline in maximum heart rate. *Proc Natl Acad Sci U S A*. 2013;110(44):18011–18016. doi:10.1073/pnas.1308477110
29. Yaniv Y, Ahmet I, Tsutsui K, et al. Deterioration of autonomic neuronal receptor signaling and mechanisms intrinsic to heart pacemaker cells contribute to age-associated alterations in heart rate variability in vivo. *Aging Cell*. 2016;15(4):716–724. doi:10.1111/acel.12483
30. Christou DD, Seals DR. Decreased maximal heart rate with aging is related to reduced (beta)-adrenergic responsiveness but is largely explained by a reduction in intrinsic heart rate. *J Appl Physiol (1985)*. 2008;105(1):24–29. doi:10.1152/jappphysiol.90401.2008
31. Craft N, Schwartz JB. Effects of age on intrinsic heart rate, heart rate variability, and AV conduction in healthy humans. *Am J Physiol*. 1995;268(4 Pt 2):H1441–H1452. doi:10.1152/ajpheart.1995.268.4.H1441
32. Mangrum JM, DiMarco JP. The evaluation and management of bradycardia. *N Engl J Med*. 2000;342(10):703–709. doi:10.1056/NEJM200003093421006
33. Adán V, Crown LA. Diagnosis and treatment of sick sinus syndrome. *Am Fam Physician*. 2003;67(8):1725–1732.
34. Alfaras I, Di Germanio C, Bernier M, et al. Pharmacological strategies to retard cardiovascular aging. *Circ Res*. 2016;118(10):1626–1642. doi:10.1161/CIRCRESAHA.116.307475
35. Takawale A, Zhang P, Patel VB, Wang X, Oudit G, Kassiri Z. Tissue inhibitor of matrix metalloproteinase-1 promotes myocardial fibrosis by mediating CD63-integrin β 1 interaction. *Hypertension*. 2017;69(6):1092–1103. doi:10.1161/HYPERTENSIONAHA.117.09045
36. Takawale A, Sakamuri SS, Kassiri Z. Extracellular matrix communication and turnover in cardiac physiology and pathology. *Compr Physiol*. 2015;5(2):687–719. doi:10.1002/cphy.c140045
37. Springer J, Azer J, Hua R, et al. The natriuretic peptides BNP and CNP increase heart rate and electrical conduction by stimulating ionic currents in the sinoatrial node and atrial myocardium following activation of guanylyl cyclase-linked natriuretic peptide receptors. *J Mol Cell Cardiol*. 2012;52(5):1122–1134. doi:10.1016/j.yjmcc.2012.01.018
38. Matsukawa N, Grzesik WJ, Takahashi N, et al. The natriuretic peptide clearance receptor locally modulates the physiological effects of the natriuretic peptide system. *Proc Natl Acad Sci U S A*. 1999;96(13):7403–7408. doi:10.1073/pnas.96.13.7403
39. Jansen HJ, Moghtadaei M, Rafferty SA, Rose RA. Atrial fibrillation in aging and frail mice: modulation by natriuretic peptide receptor C. *Circ Arrhythm Electrophysiol*. 2021;14(9):e010077. doi:10.1161/CIRCEP.121.010077
40. Yoshida Y, Nakanishi K, Daimon M, et al. Alteration of cardiac performance and serum B-type natriuretic peptide level in healthy aging. *J Am Coll Cardiol*. 2019;74(14):1789–1800. doi:10.1016/j.jacc.2019.07.080
41. Davis KM, Fish LC, Minaker KL, Elahi D. Atrial natriuretic peptide levels in the elderly: differentiating normal aging changes from disease. *J Gerontol A Biol Sci Med Sci*. 1996;51(3):M95–101. doi:10.1093/gerona/51a.3.m95

Loss of natriuretic peptide receptor C enhances sinoatrial node dysfunction in aging and frail mice

Supplementary Material

Supplemental Methods

Mouse clinical frailty assessment

Frailty was assessed in mice using the mouse clinical FI. Assessments of the integument, musculoskeletal, vestibulocochlear/auditory, ocular, nasal, digestive, urogenital and respiratory systems were performed. Signs of discomfort, body temperature and body mass were also assessed. Each item was given a score of 0 (no sign of deficit), 0.5 (mild deficit) or 1 (severe deficit). Deficits in body temperature and body mass were scored based on deviation from the mean in all mice. The scores for each item were added together and the sum was divided by the number of items measured (i.e. 31 items) to yield an FI score between 0 and 1.

***In vivo* electrophysiology**

HR was measured in anesthetized mice (2% isoflurane inhalation) using 30-gauge subdermal needle electrodes (Grass Technologies) to record body surface (lead II) ECGs. In parallel, a 1.2 French octapolar electrophysiology catheter was inserted in the right heart via the jugular vein and used for intracardiac programmed stimulation experiments. All stimulation pulses were given at 3 V for 2 ms, which enabled continuous capture and drive of cardiac conduction. Sinoatrial node recovery time (SNRT) was measured by delivering a 12-stimulus drive train at a cycle length of 100 ms. SNRT is defined as the time between the last stimulus in the drive train and the occurrence of the first spontaneous atrial beat (P wave). SNRT was

corrected for heart rate (cSNRT) by subtracting the prestimulus RR interval from the measured SNRT. Data were acquired using a Gould ACQ-7700 amplifier and Ponemah Physiology Platform software (Data Sciences International). Body temperature was monitored continuously via a rectal probe and maintained at 37°C with a heating pad.

High-resolution optical mapping

To investigate patterns of electrical conduction in the SAN we used high resolution optical mapping in atrial preparations. Hearts were excised into Krebs solution (37°C) containing (in mM): 118 NaCl, 4.7 KCl, 1.2 KH₂PO₄, 25 NaHCO₃, 1 CaCl₂, 1 MgCl₂, 11 glucose and bubbled with 95% O₂/5% CO₂ to maintain a pH of 7.4. The atrial preparation was superfused continuously with Krebs solution (37°C) bubbled with 95% O₂/5% CO₂ and allowed to equilibrate for at least 10 min. The preparation was then incubated with the voltage-sensitive dye RH-237 (15 μM; Biotium) for 15 min. After the dye incubation period, superfusion was resumed with blebbistatin (10 μM; Cayman Chemical Company) added to the superfusate to suppress contractile activity and prevent motion artifacts. Experiments were performed in sinus rhythm so that the cycle length (i.e. beating rate) of the atrial preparation was free to change. RH-237-loaded atrial preparations were illuminated with light from the X-Cite Xylis Broad Spectrum LED Illumination System (Excelitas Technologies) and filtered with a 520/35 nm excitation filter (Semrock). Emitted fluorescence was separated by a dichroic mirror (560 nm cut-off; Semrock) and filtered by a 715 nm long-pass emissions filter (Andover Corp.). Recordings were captured using a high-speed CMOS camera (MiCAM03-N256, SciMedia). We mapped conduction in the region of the right atrial posterior wall around the point of initial electrical excitation, which corresponds to the activation of the SAN. The region that was mapped

extended from the superior vena cava to the inferior cava along the edge of the crista terminalis, based on the known anatomical location of the SAN in the mouse heart. Data were captured from an optical field of view of 6.8 x 6.8 mm at a frame rate of 1000 or 3000 frames/s using BrainVision software (BrainVision Inc.). The spatial resolution was 26.6 x 26.6 μM for each pixel. Magnification was constant in all experiments and no pixel binning was used. All optical data were analyzed using custom software written in MATLAB[®] (Mathworks) as we have previously described.

Quantitative PCR

Quantitative gene expression was performed in isolated SAN tissue. Intron spanning primers for *npr3* (NPR-C), *cacna1c* (Cav1.2), *cacna1d* (Cav1.3), *hcn1* (HCN1), *hcn2* (HCN2), *hcn4* (HCN4), *coll1a* (collagen type I), *col3a* (collagen type III), *tgfb1* (transforming growth factor β), *mmp9* (matrix metalloproteinase 9), as well as *timp1*, *timp2*, *timp3* and *timp4* (tissue inhibitor of metalloproteinase 1-4) were used. *gapdh* (GAPDH) was used as a reference gene in all experiments except for *npr3* expression studies which used *hppt1* (hypoxanthine phosphoribosyltransferase 1) as a reference gene. Primer sequences are provided Supplemental Table 1. Following synthesis, primers were reconstituted in nuclease free water at a concentration of 100 μM and stored at -20°C . All primer sets were validated in order to determine optimal annealing temperature as well as confirmation of ideal amplification efficiency (between 90-110% copy efficiency per cycle). RNA was extracted in PureZOL[™] RNA isolation reagent according to kit instructions (Aurum Total RNA Fatty and Fibrous Tissue Kit, Bio-Rad). RNA was eluted in 40 μl of elution buffer from the spin column. RNA purity and quantity were determined using a NanoPhotometer (Implen). First strand synthesis reactions

were performed using the iScript cDNA synthesis kit (Bio-Rad) according to kit instructions. Lack of genomic DNA contamination was verified by reverse transcription (RT)-PCR using a no RT control. RT-qPCR using BRYT green dye (Promega) was used to assess gene expression.

Collagen staining and immunohistochemistry

Fibrosis in the SAN was assessed using picrosirius red staining on paraffin embedded sections (5 μ m) through the SAN. The myocardium was counterstained using fast green. The SAN region was confirmed using HCN4 immunostaining in adjacent sections. The level of fibrosis was quantified using ImageJ software.

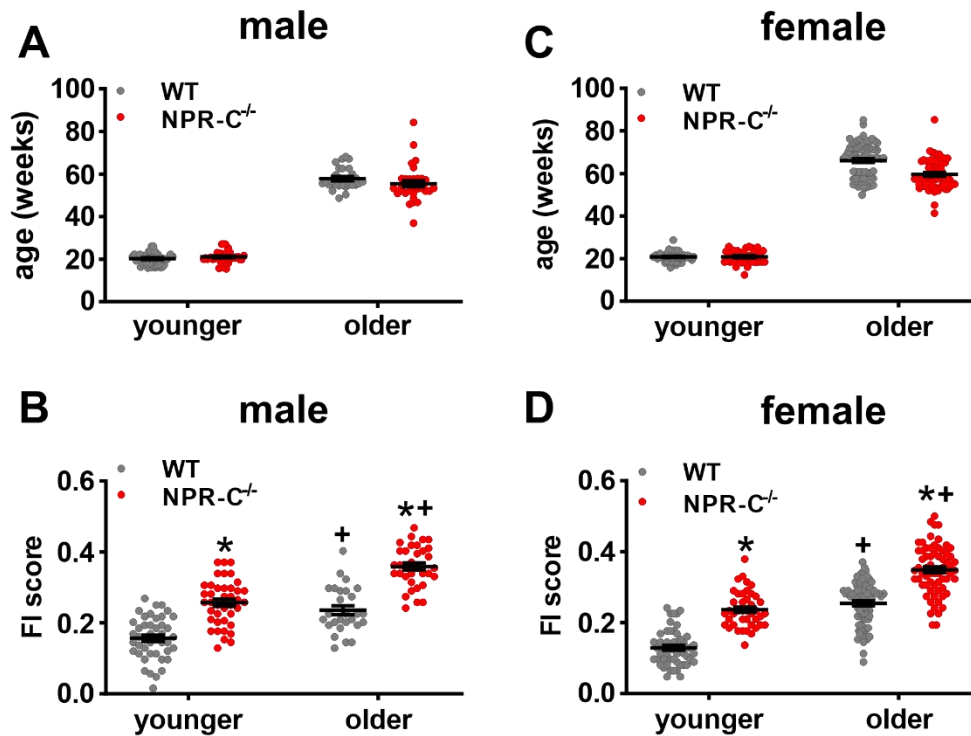
Plasma creatinine

Plasma creatinine was measured using a creatinine assay kit (Abcam) according to the manufacturer's instructions.

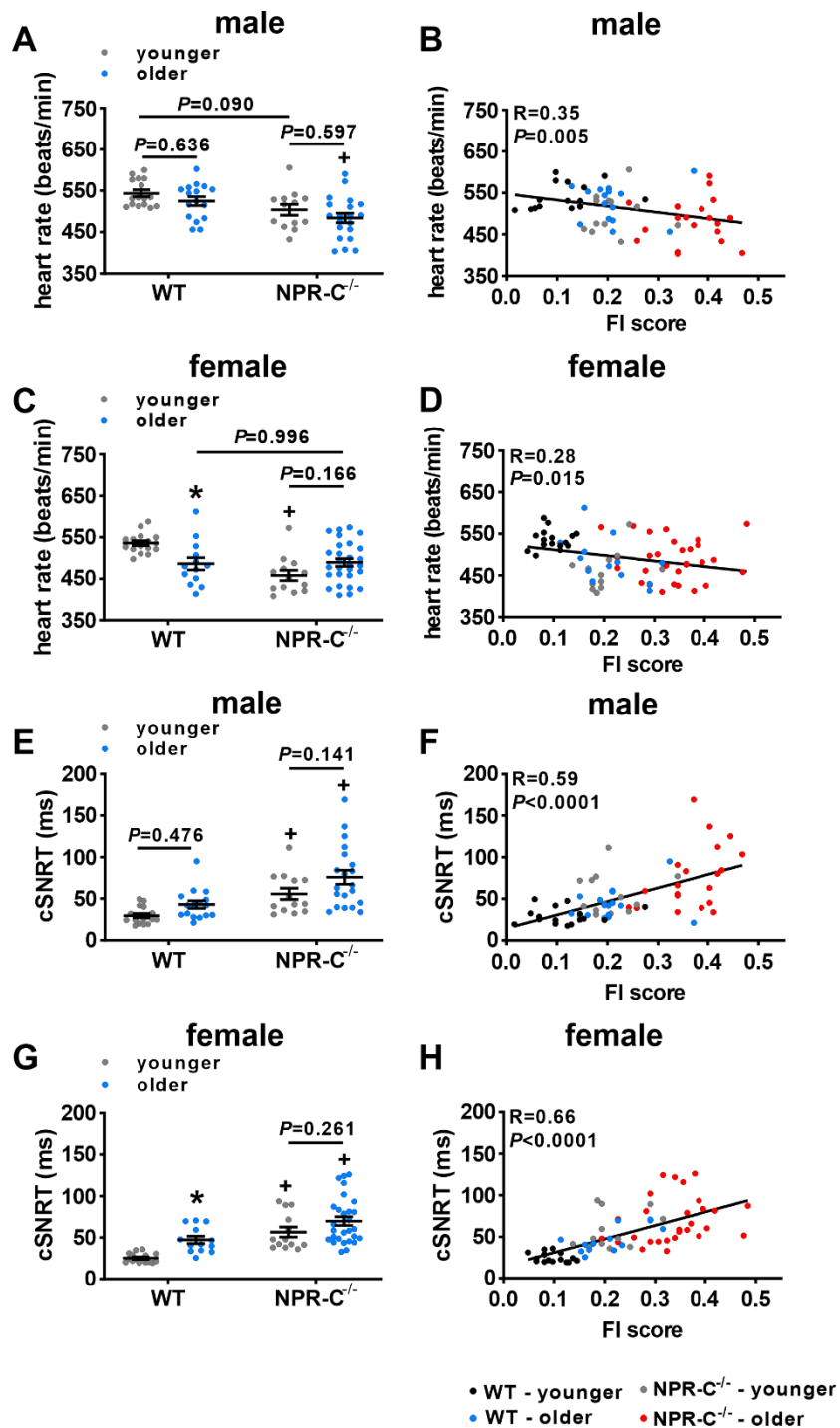
Echocardiography

Cardiac structure was assessed by echocardiography in mice anesthetized by isoflurane inhalation (2%) using a Vevo 3100 ultrasound machine (Fujifilm VisualSonics).

Supplemental Figures

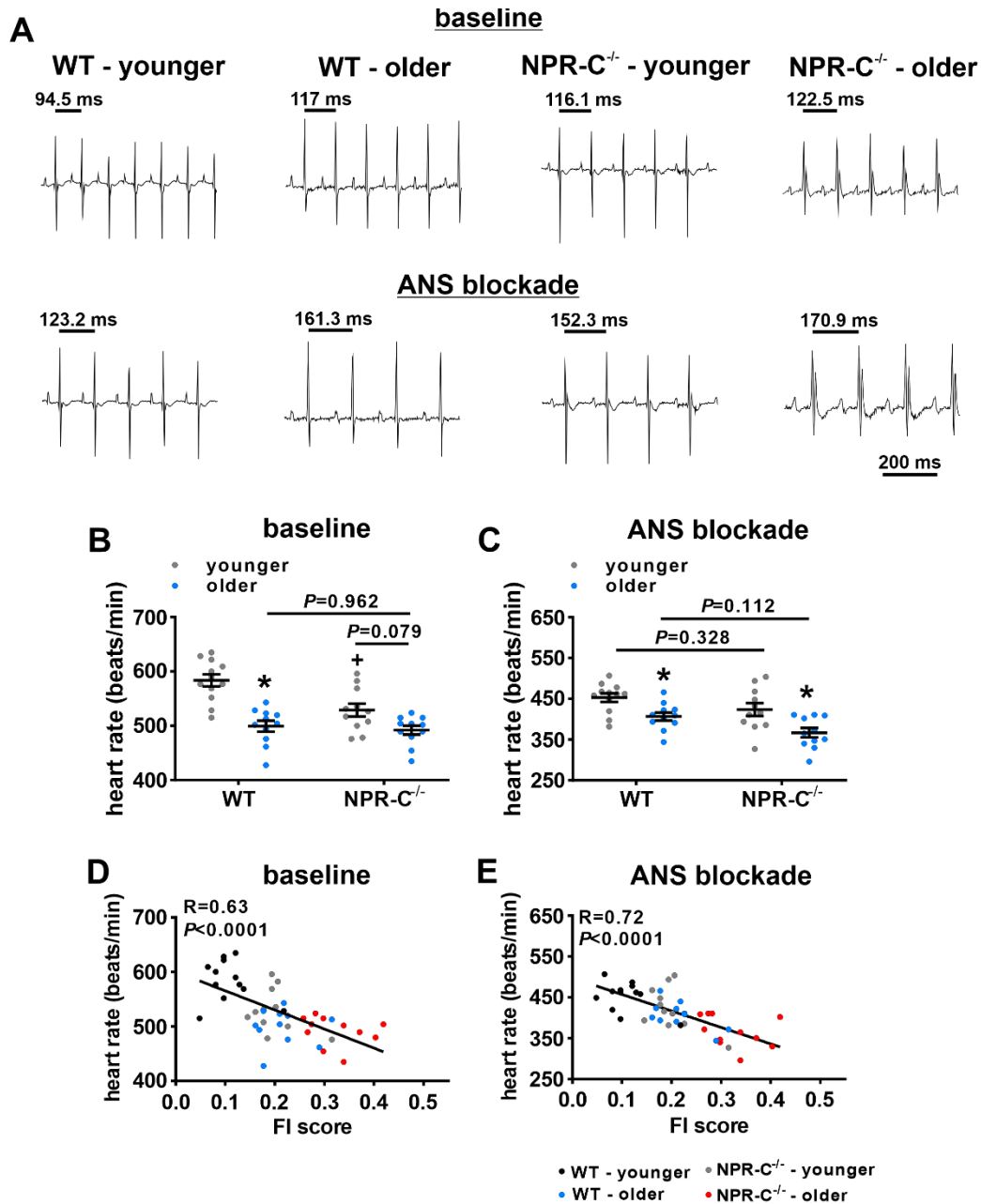


Supplemental Figure 1. Ages and frailty index scores for male and female WT and NPR-C^{-/-} mice. (A) Ages of male younger and older WT and NPR-C^{-/-} mice used in this study; $n=44$ mice for WT-younger, 27 for WT-older, 40 for NPR-C^{-/-}-younger and 34 for NPR-C^{-/-}-older. (B) Frailty index (FI) scores in male younger and older WT and NPR-C^{-/-} mice used in this study (same mice as panel A). (C) Ages of female younger and older WT and NPR-C^{-/-} mice used in this study; $n=53$ mice for WT-younger, 77 for WT-older, 42 for NPR-C^{-/-}-younger and 66 for NPR-C^{-/-}-older. (D) FI scores in female younger and older WT and NPR-C^{-/-} mice used in this study (same mice as panel C). * $P<0.05$ vs. WT, + $P<0.05$ vs. younger by two-way ANOVA with a Tukey posthoc test.

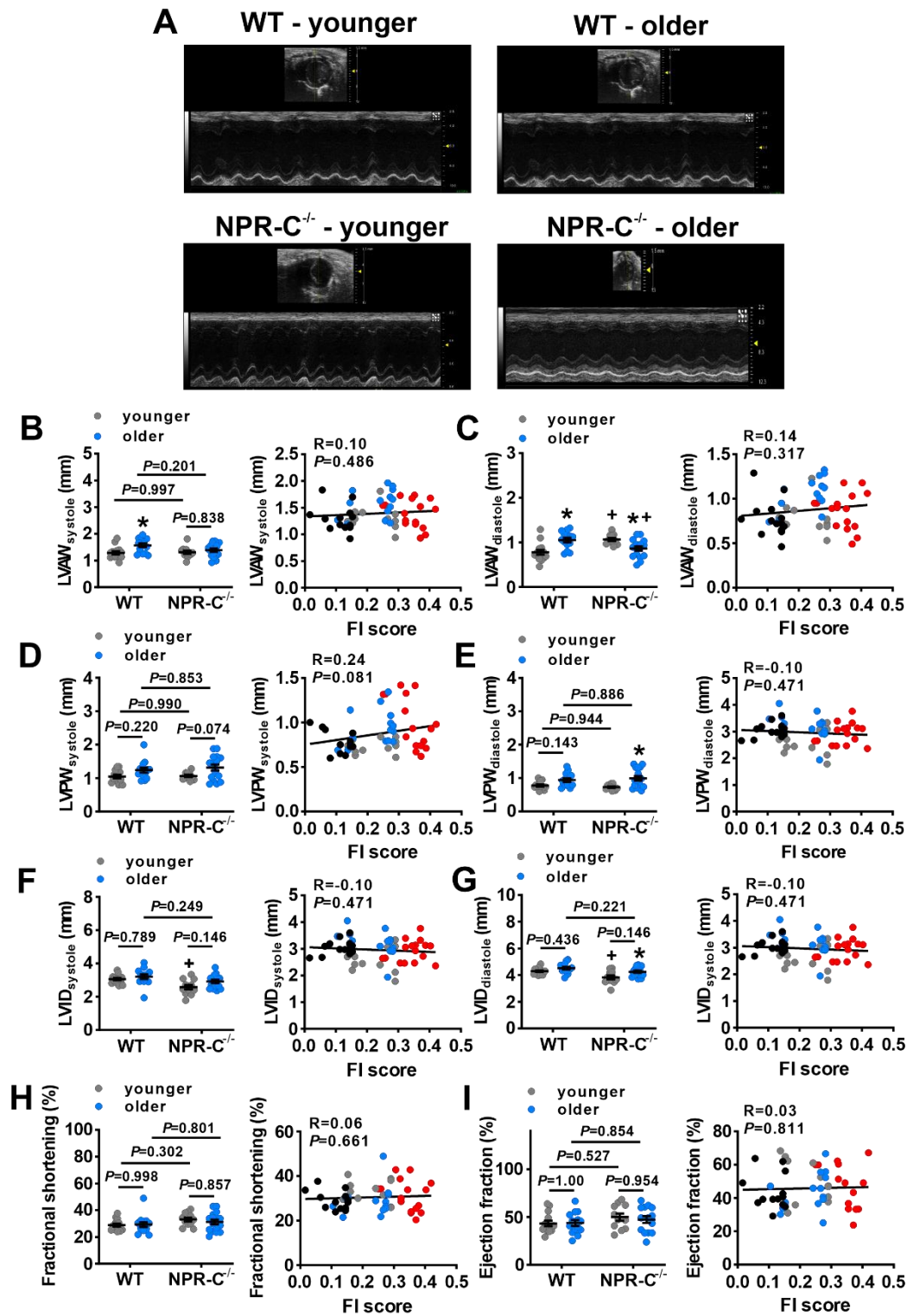


Supplemental Figure 2. Heart rate and corrected sinoatrial node recovery time in male and female WT and NPR-C^{-/-} mice. **(A)** Heart rate in male younger and older WT and NPR-C^{-/-} mice. **(B)** Heart rate in male younger and older WT and NPR-C^{-/-} mice as function of FI score (same mice as panel A). **(C)** Heart rate in female younger and older WT and NPR-C^{-/-} mice. **(D)** Heart rate in female younger and older WT and NPR-C^{-/-} mice as a function of FI score (same mice as panel C). **(E)** Corrected sinoatrial node recovery time (cSNRT) in male younger and older WT

and NPR-C^{-/-} mice. **(F)** cSNRT in male younger and older WT and NPR-C^{-/-} mice as function of FI score (same mice as panel **E**). **(G)** cSNRT in female younger and older WT and NPR-C^{-/-} mice. **(H)** cSNRT in female younger and older WT and NPR-C^{-/-} mice as function of FI score (same mice as panel **G**). For panels **A**, **C**, **E**, and **G** * $P < 0.05$ vs. younger, + $P < 0.05$ vs. WT by two-way ANOVA with a Tukey posthoc test. For panels **B**, **D**, **F**, and **H** linear regressions analyzed using Pearson's correlation. For male mice $n=16$ mice for WT-younger, 16 for WT-older, 13 for NPR-C^{-/-}-younger and 20 for NPR-C^{-/-}-older. For female mice $n=16$ mice for WT-younger, 13 for WT-older, 13 for NPR-C^{-/-}-younger and 28 for NPR-C^{-/-}-older.

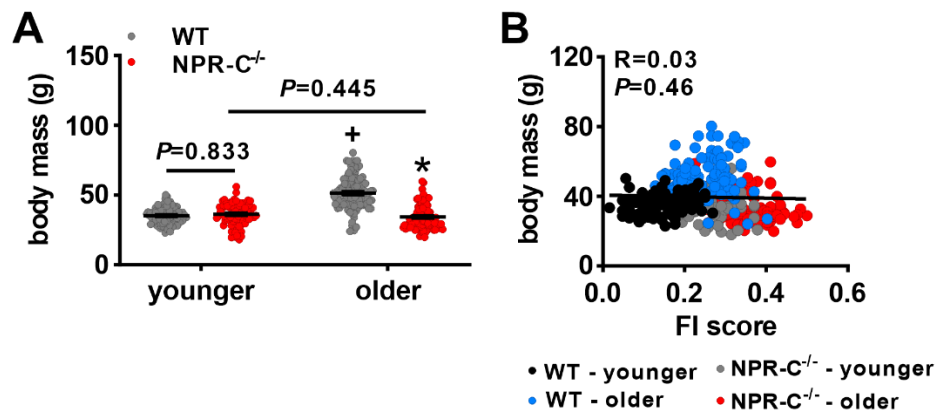


Supplemental Figure 3. Effects of age and frailty on intrinsic heart rate measured during autonomic nervous system blockade in WT and NPR-C^{-/-} mice. Autonomic nervous system (ANS) blockade was achieved by intraperitoneal injection of atropine (10 mg/kg) and propranolol (10 mg/kg). (A) Representative ECGs in younger and older WT and NPR-C^{-/-} mice at baseline and after ANS blockade. (B and C) Heart rate at baseline (B) and after ANS blockade (C) in younger and older WT and NPR-C^{-/-} mice. * $P<0.05$ vs. younger, + $P<0.05$ vs. WT by two-way ANOVA with a Tukey posthoc test; $n=12$ mice for WT-younger, 11 for WT-older, 11 for NPR-C^{-/-}-younger and 11 for NPR-C^{-/-}-older. (D and E) Heart rate at baseline (D) and after ANS blockade (E) in younger and older WT and NPR-C^{-/-} mice as function of FI score (same mice as panels B and C). Linear regressions analyzed using Pearson's correlation.

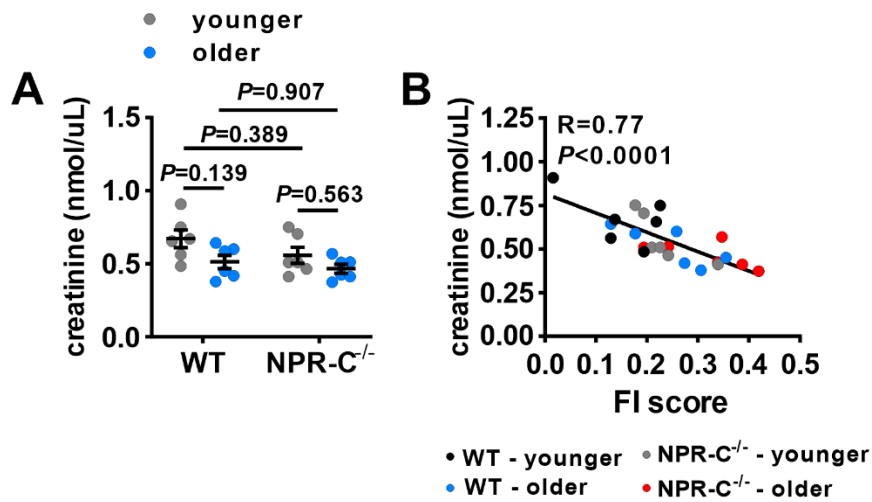


Supplemental Figure 4. Echocardiography in WT and NPR-C^{-/-} mice. (A) Representative M-mode images measured from the short axis in younger and older WT and NPR-C^{-/-} mice. (B-C) left ventricular anterior wall (LVAW) thickness in systole (B) and diastole (C) as a function of

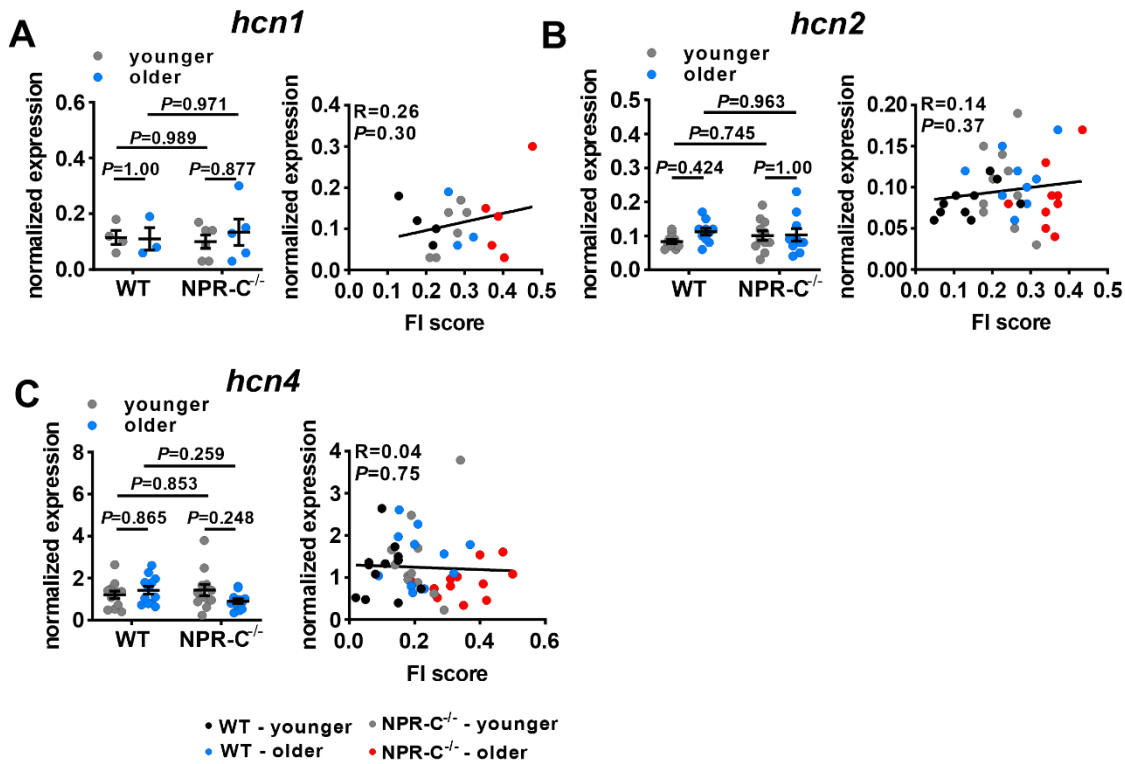
age/genotype (left) and FI score (right). **(D-E)** left ventricular posterior wall (LVPW) thickness in systole (**D**) and diastole (**E**) as a function of age/genotype (left) and FI score (right). **(F-G)** left ventricular internal diameter (LVID) in systole (**F**) and diastole (**G**) as a function of age/genotype (left) and FI score (right). **(H-I)** ejection fraction (**H**) and fractional shortening (**I**) as a function of age/genotype (left) and FI score (right). * $P < 0.05$ vs. younger, ⁺ $P < 0.05$ vs. WT by two-way ANOVA with a Tukey posthoc test. Linear regressions analyzed using Pearson's correlation. $n=14$ mice for WT-younger, 14 for WT-older, 11 for NPR-C^{-/-}-younger and 16 for NPR-C^{-/-}-older.



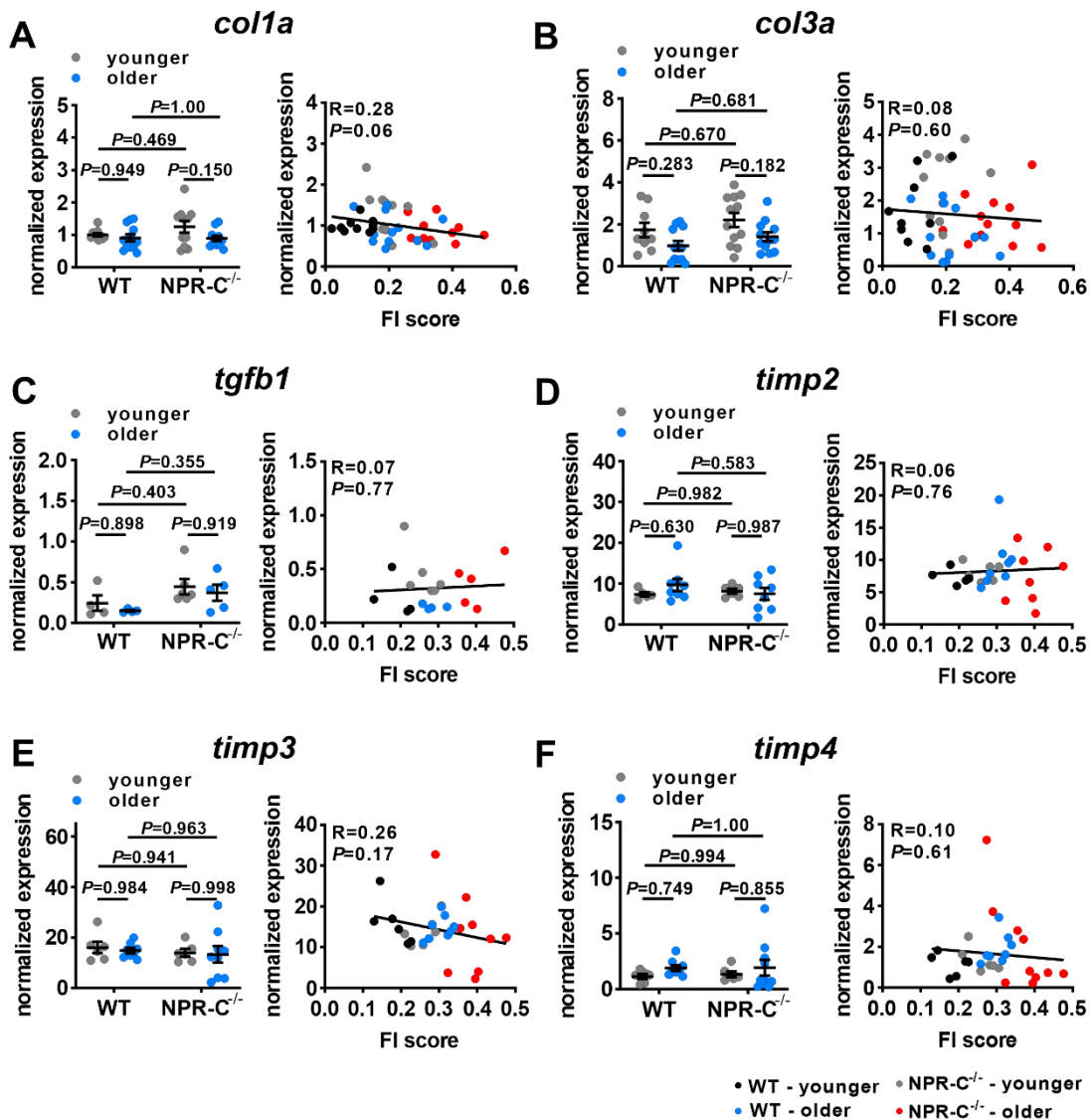
Supplemental Figure 5. Body mass in wildtype and NPR-C^{-/-} mice. **(A)** Body mass in younger and older WT and NPR-C^{-/-} mice used in this study; $n=97$ mice for WT-younger, 103 for WT-older, 82 for NPR-C^{-/-}-younger and 100 for NPR-C^{-/-}-older; * $P<0.05$ vs. WT, + $P<0.05$ vs. younger by two-way ANOVA with a Tukey posthoc test. **(B)** Body mass as a function of FI score (same mice as panel A). Linear regression analyzed using Pearson's correlation.



Supplemental Figure 6. Effects of age and frailty on plasma creatinine in WT and NPR-C^{-/-} mice. **(A)** serum creatinine in younger and older WT and NPR-C^{-/-} mice. * $P<0.05$ vs. younger, ⁺ $P<0.05$ vs. WT by two-way ANOVA with a Tukey posthoc test. **(B)** serum creatine as a function of FI score for younger and older WT and NPR-C^{-/-} mice (same mice as panel A). Linear regression analyzed using Pearson's correlation. $n=6$ mice for WT-younger, 6 for WT-older, 6 for NPR-C^{-/-}-younger and 6 for NPR-C^{-/-}-older.



Supplemental Figure 7. Effects of age and frailty on sinoatrial node HCN mRNA expression in WT and NPR-C^{-/-} mice. (A) mRNA expression of *hcn1* in younger and older WT and NPR-C^{-/-} mice (left panel) and as a function of FI score (right panel); $n=4$ mice for WT-younger, 3 for WT-older, 6 for NPR-C^{-/-}-younger and 5 for NPR-C^{-/-}-older. (B) mRNA expression of *hcn2* in younger and older WT and NPR-C^{-/-} mice (left panel) and as a function of FI score (right panel); $n=10$ mice for WT-younger, 10 for WT-older, 11 for NPR-C^{-/-}-younger and 10 for NPR-C^{-/-}-older. (C) mRNA expression of *hcn4* in younger and older WT and NPR-C^{-/-} mice (left panel) and as a function of FI score (right panel); $n=12$ mice for WT-younger, 12 for WT-older, 12 for NPR-C^{-/-}-younger and 12 for NPR-C^{-/-}-older. For figures as a function of chronological age and genotype * $P<0.05$ vs. younger; [†] $P<0.05$ vs. WT by two-way ANOVA with a Tukey posthoc test. For figures as a function of FI score linear regressions analyzed using Pearson's correlation.



Supplemental Figure 8. Effects of age and frailty on mRNA expression of profibrotic genes in the sinoatrial node in WT and NPR-C^{-/-} mice. **(A)** mRNA expression of *col1a* in younger and older WT and NPR-C^{-/-} mice (left panel) and as a function of FI score (right panel); $n=10$ mice for WT-younger, 12 for WT-older, 11 for NPR-C^{-/-}-younger and 11 for NPR-C^{-/-}-older. **(B)** mRNA expression of *col3a* in younger and older WT and NPR-C^{-/-} mice (left panel) and as a function of FI score (right panel); $n=9$ mice for WT-younger, 12 for WT-older, 12 for NPR-C^{-/-}-younger and 12 for NPR-C^{-/-}-older. **(C)** mRNA expression of *tgfb1* in younger and older WT and NPR-C^{-/-} mice (left panel) and as a function of FI score (right panel); $n=4$ mice for WT-younger, 4 for WT-older, 6 for NPR-C^{-/-}-younger and 5 for NPR-C^{-/-}-older. **(D)** mRNA expression of *timp2* in younger and older WT and NPR-C^{-/-} mice (left panel) and as a function of FI score (right panel); $n=5$ mice for WT-younger, 8 for WT-older, 6 for NPR-C^{-/-}-younger and 8 for NPR-C^{-/-}-older. **(E)** mRNA expression of *timp3* in younger and older WT and NPR-C^{-/-} mice (left panel) and as a function of FI score (right panel); $n=6$ mice for WT-younger, 8 for WT-older, 6 for NPR-C^{-/-}-younger and 9 for NPR-C^{-/-}-older. **(F)** mRNA expression of *timp4* in younger and older WT and NPR-C^{-/-} mice (left panel) and as a function of FI score (right panel); $n=6$ mice for

WT-younger, 8 for WT-older, 6 for NPR-C^{-/-}-younger and 10 for NPR-C^{-/-}-older. For figures as a function of chronological age and genotype * $P < 0.05$ vs. younger; + $P < 0.05$ vs. WT by two-way ANOVA with a Tukey posthoc test. For figures as a function of FI score linear regressions analyzed using Pearson's correlation.

Supplemental Table 1: Quantitative PCR primers

Gene of Interest	Forward Primer (5' → 3')	Reverse Primer (3' → 5')	Amplicon Length
<i>Npr3</i>	CGAGCGAGTGGTGATCATGTGTG	CTCCACGAGCCATCTCCGTAGG	147
<i>Cacna1c</i>	ATGATTCGGGCCTTTGTTTCAG	TGGAGTAGGGATGTGCTCG	228
<i>Cacna1d</i>	TGAAGGAGAAGATTGCGCCC	TTGCGGAATGAGTGGCTACG	190
<i>Hcn1</i>	CTCTTTTGTCTAACGCCGAT	CATTGAAATGTCCACCGAA	291
<i>Hcn2</i>	CTTCACCAAGATCCTCAGTCTG	GGTCGTAGGTCATGTGGAAA	92
<i>Hcn4</i>	CCAGGAGAAGTATAAACAGGTGGAGCG	GTTGATGATCTCCTCTCGAAGTGGCTC	169
<i>Colla</i>	GCGGACTCTGTTGCTGCTTGC	GACCTGCGGGACCCCTTTGT	125
<i>Col3a</i>	AGATCCGGGTCTCCTGGCATT	CTGGTCCCGGATAGCCACCCAT	194
<i>Tgfb1</i>	CGAGGTGACCTGGGCACCATCCATGAC	CTGCTCCACCTTGGGCTTGCACCCAC	405
<i>Mmp9</i>	TCGCGTGGATAAGGAGTTCTC	ATGGCAGAAATAGGCTTTGTCTTG	82
<i>Timp1</i>	CAGATACCATGATGGCCCCC	CGCTGGTATAAGGTGGTCTCG	190
<i>Timp2</i>	CCAGAAGAAGAGCCTGAACCA	GTCCATCCAGAGGCACTCATC	112
<i>Timp3</i>	GGCCTCAATTACCGCTACCA	CTGATAGCCAGGGTACCCAAAA	135
<i>Timp4</i>	TGCAGAGGGAGAGCCTGAA	GGTACATGGCACTGCATAGCA	180
<i>gapdh</i>	CACCCTTCAAGTGGGCCCCG	CACCCTTCAAGTGGGCCCCG	227
<i>Hprt1</i>	GCAGGTCAGCAAAGAACTTATAGCC	CTCATGGACTGATTATGGACAGGAC	123